Since January 2020 Elsevier has created a COVID-19 resource centre with free information in English and Mandarin on the novel coronavirus COVID-19. The COVID-19 resource centre is hosted on Elsevier Connect, the company's public news and information website.

Materials Science & Engineering C 107 (2020) 110308

Contents lists available at ScienceDirect

Materials Science & Engineering C

journal homepage: www.elsevier.com/locate/msec

Fabrication of silk fibroin/poly(lactic-co-glycolic acid)/graphene oxide microfiber mat via electrospinning for protective fabric

Zulan Liu[a,b,c], Songmin Shang[a,*], Ka-lok Chiu[a], Shouxiang Jiang[a], Fangyin Dai[c]

[a] Institute of Textiles and Clothing, The Hong Kong Polytechnic University, Hong Kong
[b] Chongqing Engineering Research Center of Biomaterial Fiber and Modern Textile, College of Textile and Garment, Southwest University, Chongqing, 400715, China
[c] State Key Laboratory of Silkworm Genome Biology, Key Laboratory of Sericultural Biology and Genetic Breeding, Ministry of Agriculture, Southwest University, Chongqing, 400715, China

ARTICLE INFO

Keywords:
Microfiber mat
Silk fibroin
poly(lactic-co-glycolic acid)
Graphene oxide
Electrospinning
Physical property
Protective fabric

ABSTRACT

In this study, a biodegradable silk fibroin/poly(lactic-co-glycolic acid)/graphene oxide (SF/PLGA/GO) microfiber mat was successfully fabricated via electrospinning for use in protective fabrics. The morphology of the microfiber mat was characterized by Scanning Electron Microscope (SEM). The thermal and mechanical properties, water contact angle, surface area and pore size of the microfiber mats were characterized. Due to the introduction of graphene which can interact with silk fibroin, the SF/PLGA/GO microfiber mat, compared with the silk fibroin/poly (lactic-co-glycolic acid) (SF/PLGA) microfiber mat, has higher strength, greater Young's modulus and better thermal stability which can meet the requirements of protective fabric. The microfiber mat is biodegradable because its main component is silk fibroin and PLGA. In particular, the microfiber mat has a small pore size range of 4 ~ 10 nm in diameter, a larger surface area of 2.63 $m^2 g^{-1}$ and pore volume of 7.09 × 10^{-3} $cm^3 g^{-1}$. The small pore size of the mat can effectively block the particulate pollutants and pathogenic particles in the air. The larger surface area and pore volume of the mat are effective for breathability. Therefore, the fabricated SF/PLGA/GO microfiber mat has great application potentials for protective fabrics.

1. Introduction

In recent years, poor air quality [1,2], rapid spread of epidemics [3], and non-biodegradable polymers [4] have become the most serious environmental problems worldwide. The air-borne fine particulate pollutants, such as fine particulate matter ($PM_{2.5}$), and various pathogens (such as avian influenza), may cause respiratory infections or illness [5]. The non-biodegradable polymers have caused serious environmental impacts. The conventional protective textiles composed of micron-sized fibers, such as cotton fibers, are incapable of filtering fine particulate pollutants such as $PM_{2.5}$, owing to their relatively large pore size. It also doesn't possess the ability to filter various pathogenic particles. Thanks to the emergence of simple and effective sub-micron fiber fabricating technique - electrospinning [6], the development of electrospun protective textiles has attracted a lot of interest from researchers. Many polymer materials, such as polyimide (PI) [7], polyurethane (PU) [8], polyacrylonitrile (PAN) [9], polyamide-66 (PA-66) [10], and some other polymers have been successfully fabricated as nanofibrous membranes for filtration. However, these polymers are pure synthetic fibers which are difficult to biodegrade after use which can cause the serious environmental problem. Therefore, the challenge is critical urgent to fabricate a protective fabric which has better filterability to effectively barrier to particulate pollutants and pathogenic particles, and has good biodegradability to avoid generation of non-degradable contaminants after use. In this work, we are committed to developing a biodegradable protective fabric with good filterability and good strength that can be used to protect individuals effectively from particulate pollutants and pathogenic particles.

Through fabricating microfibers by electrospinning, the desired properties and functions can be obtained by manipulating fiber composition [11]. Various polymers have been prepared by electrospinning for various purpose [12], and the demands for electrospun polymers are gradually increasing with the rapid growth of living needs and technological development [13,14]. The applications of microfiber materials include tissue engineering, biosensors, filtration, and wound dressings due to their high surface area to volume ratio and tunable porosity [15–17].

Bombyx mori (silkworm) silk is a naturally renewable material with easy degradation, good biocompatibility [18], and excellent mechanical performance [19], which can be processed into various formats

* Corresponding author.
E-mail address: shang.songmin@polyu.edu.hk (S. Shang).

https://doi.org/10.1016/j.msec.2019.110308
Received 24 August 2019; Received in revised form 11 October 2019; Accepted 11 October 2019
Available online 22 October 2019
0928-4931/

[20–22]. One form of regenerated silk fibroin is a microfiber which has been the research hotspot since nanotechnology emerged [23,24]. However, the spinnability of regenerated silk fibroin is poor. The introduction of polymers is an effective way to improve the spinnability of regenerated silk fibroin. Poly(lactic-co-glycolic acid) (PLGA) with excellent biocompatibility and biodegradability has been widely used to form electrospun microfibers and is applied to FDA-approved biomaterials. Therefore, the PLGA was chosen to improve the spinnability of the regenerated silk fibroin.

As a natural protein fiber, silk is mainly composed of alanine, glycine and serine, which offer reactive functional groups on the side chains of silk [18,25,26]. The functional groups in silk macromolecules are likely react with reactive groups in other materials under certain conditions to obtain composites [27,28]. Graphene oxide (GO) is a single layer of carbon atoms having functional hydroxyl, epoxide, diol, and carbonyl groups [29–31]. These functional groups endow some unique properties to graphene oxide, such as excellent hydrophilicity, dispersibility and biocompatibility [32–34]. GO with a higher specific surface area and abundant functional groups has wide applications in cell adhesion, reinforcing material and antibacterial activity [35,36]. GO can easily form hydrogen bonds with the hydrophilic amide groups in silk fibroin (SF) because GO contains lots of oxygen functional groups [37,38].

In this study, we fabricated a silk fibroin/poly(lactic-co-glycolic acid)/graphene oxide (SF/PLGA/GO) microfiber mat by electrospinning for protective fabrics. The basic physical properties of the prepared mat were tested and demonstrated. Based on the naturally rich and sustainable silk fibroin, mats having different surface functions and desired properties can be easily reconstructed and prepared by designing and manipulating the components of the fiber composition. Finally, a protective fabric microfiber mat that can effectively block particulate pollutants and pathogenic particles in the air was fabricated.

2. Experimental

2.1. Materials

Regenerated silk fibroin (SF) was purchased from Huzhou Xintiansi Bio-tech Co., Ltd. Poly(lactic-co-glycolic acid) (PLGA) was purchased from Jinan Daigang Biomaterial Co., Ltd. (PLA50: PGA50, molecular weight 10K Da). 1,1,1,3,3,3-Hexafluoro-2-propanol (HFIP) (99.5%) was purchased from Aladdin. Graphene oxide (GO) was purchased from XFNANO, INC (Nanjing) using the modified Hummers' method.

2.2. Fabrication of microfiber mat by mixed electrospinning

The fabrications of SF/PLGA and SF/PLGA/GO mat consist of two steps.

The first step is to prepare a spinning solution, including SF/PLGA and SF/PLGA/GO spinning solution. An SF/PLGA spinning solution was prepared by mixing regenerated silk fibroin (0.5 g) and PLGA (0.5 g) in 9 g of 1,1,1,3,3,3-Hexafluoro-2-propanol (HFIP). The SF/PLGA/GO spinning solution was prepared by the following method: 1. Graphene oxide (0.5%, w/w) was evenly dispersed in HFIP by ultrasonic treatment for 60 min and then magnetically stirred at room temperature. 2. Regenerated silk fibroin (5%, w/w) and PLGA (5% w/w) were then separately added to the above solution and under magnetic stirring for 4 h at room temperature.

The second step is a hybrid electrospinning. The electrospinning used a high-voltage power supply unit (TL-Pro, Shenzhen, China) at a voltage of -2 kV–16 kV. The electrospinning flow rate was 1.45 ml/h to 1.50 ml/h, and the microfibers were received on the collector which was rotated at 600 rpm, 7 cm from the positively-charged spinneret, and rotated for about 5 h. The spinning temperature was 23 °C ~ 24 °C and the relative humidity was 63% ~ 68%. The volume of syringe used in the experiment was 10 ml, and the number of metal needles was No. 17th, with an inner diameter of 1.23 mm and an outside diameter of 1.5 mm. After the electrospinning, the aluminum foil with the formed mat was taken out from the collector immediately and placed in a hood for 24 h to remove residual organic solvent and moisture.

2.3. Characterization of microfiber mat

The morphology of ultrafine fibers was examined by a Scanning Electron Microscopy (TM3000, Table-Top Scanning Electron Microscope). SEM images were analyzed by Nano Measurer 1.2 Software to determine the diameter distribution of the fibers. The characterization of the molecular structure of the nanofibers was carried out by Fourier Transform Infrared (FT-IR Spectrometer, Spectrum 100, PerkinElmer). The surface chemical properties of the nanofibers were evaluated by their hydrophilicity, which was measured by an Optical Contact Angle Measuring Instrument (SDC-350). The surface area and pore size characteristics of the composites were analyzed by surface area & pore size analyzer (NOVA touch LX^4, Quantachrome Instruments). The pore size distribution (PSD) curve of the composite was retrieved with the Barrette-Joynere-Halenda (BJH) model by using the desorption branch. Raman Spectroscopy (BaySpec's 3-in-1 Nomadic™ Raman microscope) was used to determine the changes that may occur at the molecular level. The mechanical properties of the mat were measured on a universal tensile tester (INSTRON) at 25 °C and 65 ± 5% RH according to ASTM D882. Prior to the tensile test, all samples were placed in a room at temperature 25 °C and a relative humidity of 65% for 24 h. The mat was cut into strips of size 50 mm × 10 mm (tested six times per sample). The gauge length and the crosshead speed were set at 20 mm and 10 mm/min, respectively. The potential drug-carrying of the microfiber mat was carried out by the adsorption capacity for Reactive Dye Red 261 as recorded by a UH5300 Spectrophotometer.

3. Results and discussion

3.1. Morphologies and structures

The optical photographs of SF/PLGA and SF/PLGA/GO mats are shown in Fig. 1(a) -1(b). It is obvious that the surfaces of these mats are smooth. Fig. 1(b) shows that the distribution of graphene oxide in the mat is uniform. The SEM images of SF/PLGA and SF/PLGA/GO mats are shown in Fig. 1(c) – 1(d), and the fiber diameter distributions of these mats are shown in Fig. 1(e) - 1(f). Clearly, the SF/PLGA and SF/PLGA/GO mats exhibit a porous three-dimensional nonwoven structure a random orientation and a smooth surface. The diameter of the SF/PLGA maintains a relatively wide distribution range with a mean diameter of 1.22 μm. After the additoin of GO to the SF/PLGA solution, the mean diameter of the PLGA/SF/GO microfibers was decreased from 1.22 μm to 1.04 μm. The reduction in fiber diameter can be explained by the change in the properties of the electrospinning solutions caused by the addition of GO [39].

3.2. Contact angle analysis

The water wettability of the microfiber mats was evaluated using an optical contact angle meter as shown in Fig. 2(a) -2(b). The water contact angle of the SF/PLGA mat is 85.93°. While the water contact angle of the SF/PLGA/GO mat increases to 93.7°. This is because GO is an amphiphilic molecule and is less hydrophilic than SF. When GO is uniformly dispersed in SF/PLGA composite, an increase in the contact angle is caused. Obviously, GO can play an important role in adjusting the hydrophilicity of SF/PLGA mat.

3.3. FT-IR analysis

The molecular structures of the microfibers were characterized by

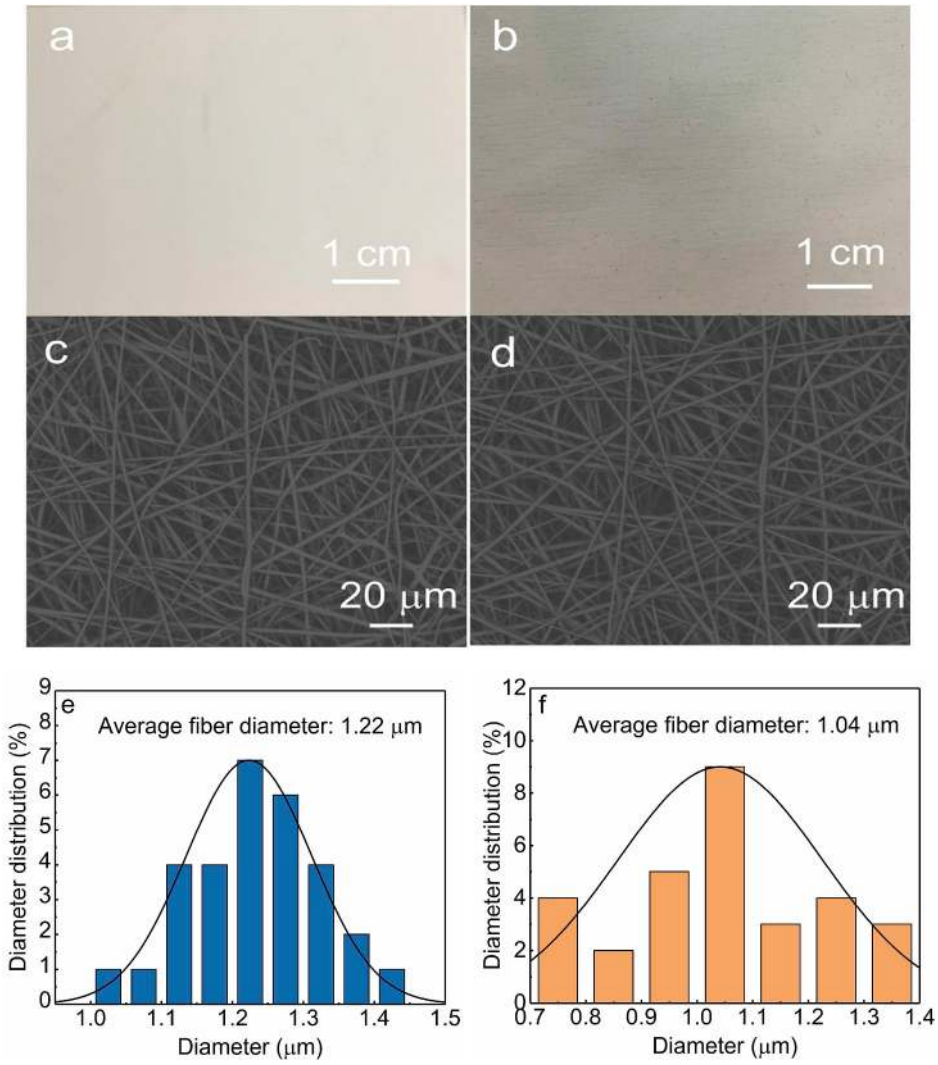

Fig. 1. The optical photographs of the SF/PLGA mat (a) and the SF/PLGA/GO mat (b); the SEM images of SF/PLGA mat (c) and SF/PLGA/GO mat (d); and the fiber diameter distributions of SF/PLGA (e) and SF/PLGA/GO (f), respectively.

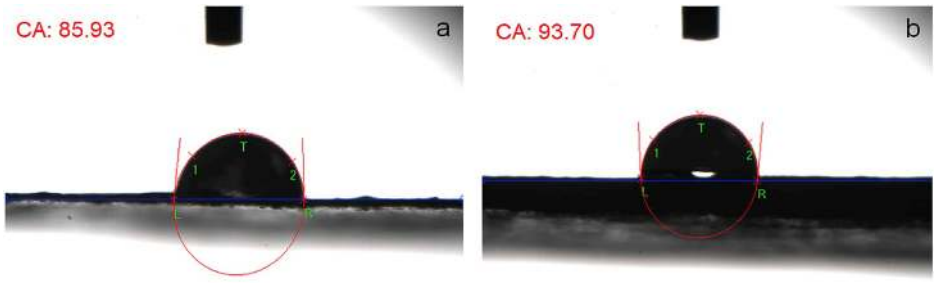

Fig. 2. The contact angles of SF/PLGA mat (a) and SF/PLGA/GO mat (b).

Fourier transform Infrared (Fig. 3). The peak assigned to C=O is 1752 cm^{-1}, and the clearly visible peaks assigned to C-O are 1170 cm^{-1} and 1084 cm^{-1}, which are the characterized peaks of PLGA [40]. These characterized PLGA peaks are shown in all spectra. There are no obvious differences in the spectra of SF/PLGA and SF/PLGA/GO. It is known that the ranges of 1700–1600 cm^{-1} (amide I), 1600–1500 cm^{-1} (amide II), and 1350–1200 cm^{-1} (amide III) are used to analyze different secondary structures of silk fibroin [41,42]. The peaks of 1647 cm^{-1} (amide I), 1545 cm^{-1} (amide II), 1266 cm^{-1} (amide III) are observed in the IR spectra of SF/PLGA and SF/PLGA/GO which are assigned to random coil-structures [43]. The peak at 1530 cm^{-1} belongs to β-sheet [44,45]. These data indicate that each component has no chemical interaction with others' components.

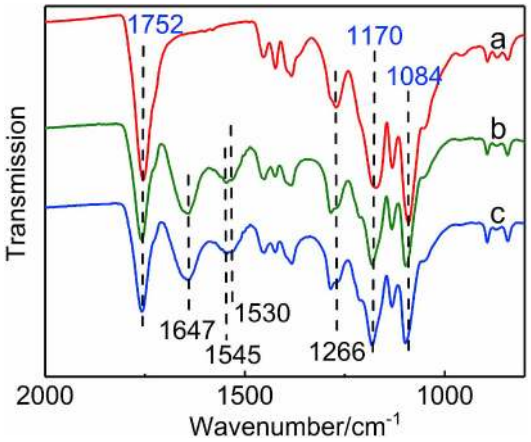

Fig. 3. FT-IR spectra of PLGA (a), SF/PLGA (b) and SF/PLGA/GO (c).

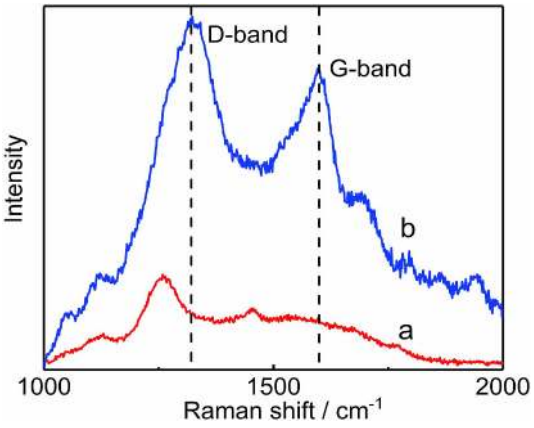

Fig. 4. Raman spectra of SF/PLGA microfiber mat (a) and SF/PLGA/GO microfiber mat (b).

3.4. Raman spectra of microfiber mat

Raman spectroscopy is useful for studying the vibrational properties and microstructure of graphite crystals and various disordered graphite materials [46]. In order to confirm the mixture of GO in the SF/PLGA microfibers, the Raman spectra were recorded. The D-band and G-band of carbon are contained in the typical Raman spectra of graphene derivative materials, including graphene oxide (GO), reduced graphene oxide (rGO), and etc. [47]. The D-band between 1330 cm^{-1} and 1340 cm^{-1} is due to the defect-activated breathing modes of the six-membered carbon rings, and the G band (1580 - 1600 cm^{-1}) is assigned to the E_{2g} phonons at the Brillouin zone center [48]. In Fig. 4, the Raman spectrum of SF/PLGA/GO exhibits two prominent peaks around 1330 cm^{-1} and 1590 cm^{-1}, which are attributed to the D-band and the G-band, respectively, indicating that GO is incorporated into the mat [49].

Table 1
Mechanical properties of the mats of SF/PLGA and SF/PLGA/GO.

Sample	Average ultimate tensile strain (%)	Average ultimate tensile stress (MPa)	Average Young's modulus (MPa)
SF/PLGA	16.40	2.42	151.99
SF/PLGA/GO	8.65	3.71	158.66

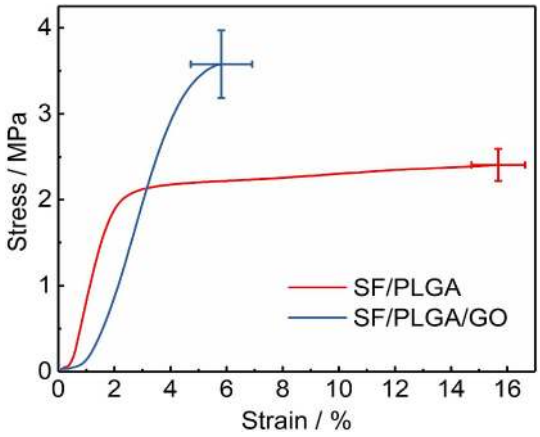

Fig. 6. The stress-strain curves of SF/PLGA mat and SF/PLGA/GO mat.

3.5. Thermogravimetric analysis (TGA)

As shown in Fig. 5(a), the thermal properties of SF/PLGA mat and SF/PLGA/GO mat were investigated by thermalgravimetric analysis. The onset temperatures of SF/PLGA mat and SF/PLGA/GO mat were 244 °C and 263 °C, respectively. It can be seen that the onset temperature of SF/PLGA/GO mat is higher compared to that of SF/PLGA. Furthermore, the mass remaining of the SF/PLGA/GO mat is also larger than the SF/PLGA mat. This result is due to the introduction of GO which has good thermal stability [50,51]. The DTG curves (Fig. 5(b))

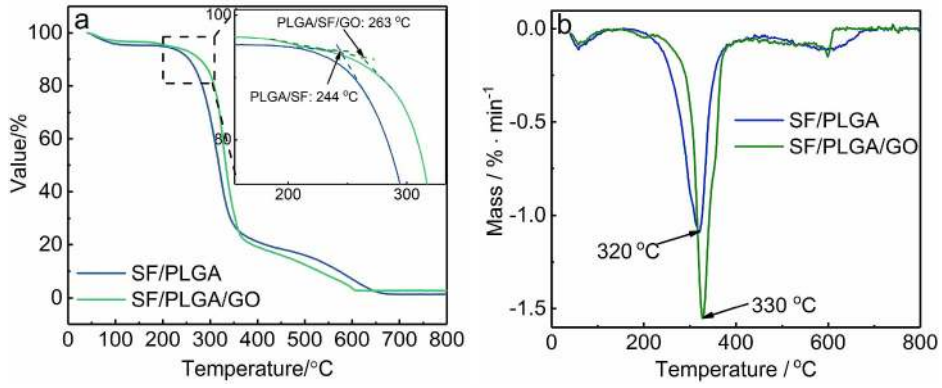

Fig. 5. TG (a) and DTG (b) curves of SF/PLGA mat and SF/PLGA/GO mat.

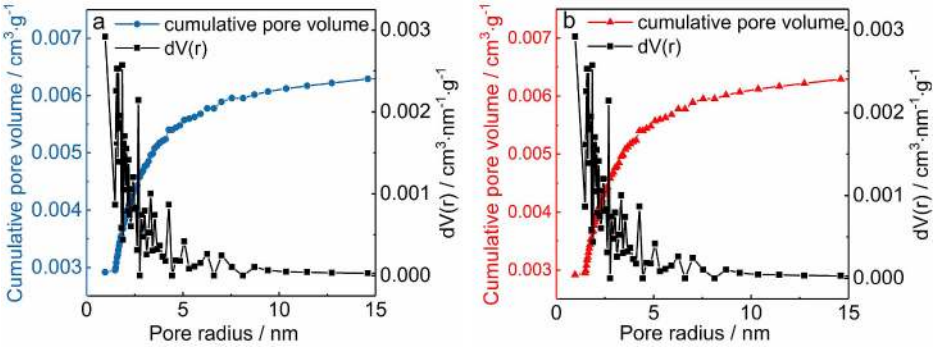

Fig. 7. Pore size distributions of SF/PLGA mat (a) and SF/PLGAGO mat (b).

show the temperatures of the maximum mass loss rate occur at 320 °C and 330 °C respectively. This is consistent with the results of thermogravimetric analysis [51,52].

3.6. Mechanical properties of the microfiber mats

The mechanical properties of the mats are listed in Table 1. The ultimate stress, ultimate strain and Young's modulus of the SF/PLGA are measured to be 2.42 MPa, 16.40% and 151.99 MPa, respectively. By adding the GO component to the SF/PLGA, the ultimate stress increases significantly to 3.71 MPa, an increase of 53%. Young's modulus increases to 158.66 MPa. This trend is common for composites which contain nanoscale reinforcing components with good dispersion and form strong interfacial interactions [53,54]. The stress-strain curves of SF/PLGA mat and SF/PLGA/GO mat are shown in Fig. 6. Both of SF/PLGA and SF/PLGA/GO mats are destroyed by breaking all the microfibers at one point, leading to a brittle failure of the strong interaction between fibers [55]. It is noted that the elongation of SF/PLGA/GO mat is lower than that of SF/PLGA mat. It is partly because of the addition of GO and forming a strong interaction with SF [56]. Compared with the SF/PLGA mat, the ultimate stress and Young's modulus of the SF/PLGA/GO mat are increased from 2.42 MPa to 3.71 MPa and 151.99 MPa to 158.66 MPa, respectively. This indicates that the mat has sufficient toughness to meet the requirements of protective fabrics.

3.7. Surface area and pore size analysis

The surface area and pore size characteristics of SF/PLGA mat and SF/PLGA/GO mat were further recorded by Surface Area & Pore Size Analyzer. A pore having an opening diameter exceeding 50 nm is referred to as a “macropore”, and a pore between 2 - 50 nm is referred to as a “mesopore”. The term “micropore” describes a pore having a diameter not exceeding 2 nm [62]. Obviously, both the pore sizes of the SF/PLGA mat and the SF/PLGAGO mat are mainly distributed in the micropores and mesopores, as shown in Fig. 7. The surface areas and pore volume characteristics of SF/PLGA and SF/PLGA/GO are listed in Table 2. The surface area and pore volume of the SF/PLGA mat are $1.14\ m^2\ g^{-1}$ and $4.45 \times 10^{-3}\ cm^3\ g^{-1}$, respectively. The surface area and pore volume of the SF/PLGA/GO mat increase with the addition of GO. It owes to the reduction of fiber diameter.

The pore sizes of SF/PLGA/GO mat are distributed in 4–10 nm (Fig. 7 & Table 3). The water vapor molecules have a diameter of 0.282 nm (Table 3), which is much smaller than the size of the mat, and can easily pass through the mat, indicating that the mat has very good vapor permeability.

Table 2
Surface areas and pore volume characteristics of SF/PLGA mat and SF/PLGA/GO mat.

Sample	$S_{BET}/m^2 \cdot g^{-1}$ [a]	$V_{total}/cm^3 \cdot g^{-1}$ [b]	$V_{micro}/cm^3 \cdot g^{-1}$ [c]	$V_{meso}/cm^3 \cdot g^{-1}$ [d]
SF/PLGA mat	1.14	4.45×10^{-3}	2.25×10^{-5}	3.85×10^{-3}
SF/PLGA/GO mat	2.63	7.09×10^{-3}	8.66×10^{-5}	5.37×10^{-3}

[a] Total surface area calculated using the BET method.
[b] Total pore volume calculated at $P/P_0 = 0.99$.
[c] Mesopore volume was calculated at $P/P_0 = 0.10$.
[d] Mesopore volume was calculated as the difference between the pore volume at P/P0 = 0.95 and P/P0 = 0.10.

The sizes of common pathogenic particles are also shown in Table 3. Their sizes are much larger than the pore sizes of the SF/PLGA/GO mat, and even much larger than the maximum size of the mat, and therefore these pathogenic particles cannot pass through the mat. In particular, the larger surface area and pore volume of the SF/PLGA/GO mat make it more resistant to pathogenic microorganisms without hindering the smooth passage of water vapor. The diameter of water droplets is 100 μm, which confirms that the prepared mat had a certain water

Table 3
Comparison between the pore sizes of the prepared mats and the sizes of particulate pollutants and pathogenic particles.

Objects	Sizes
Pore size of the SF/PLGA/GO microfiber mat	4 ~ 10 nm in diameter
Water vapor molecule	0.282 nm in diameter [57]
Water droplet	100 μm in diameter [58]
particulate pollutants ($PM_{2.5}$)	< 2.5 μm [4]
Severe acute respiratory syndrome (SARS)	80 nm [59]
Influenza A virus subtype H5N1	80 ~ 120 nm [60]
Influenza A virus subtype H7N9	80 ~ 120 nm [60]
Influenza A virus subtype H1N1	80 ~ 120 nm [60]
Staphylococcus aureus	0.8 μm [61]
Escherichia coli	2.0 μm long, 0.25 ~ 1.0 μm in diameter [61]
Salmonella	0.7 ~ 1.5 mm in diameter, lengths from 2 to 5 μm [61]
Pseudomonas aeruginosa	0.5 ~ 0.8 μm in diameter, lengths from 1.5 ~ 3 μm [61]
Candida albicans	3 ~ 6 μm [61]

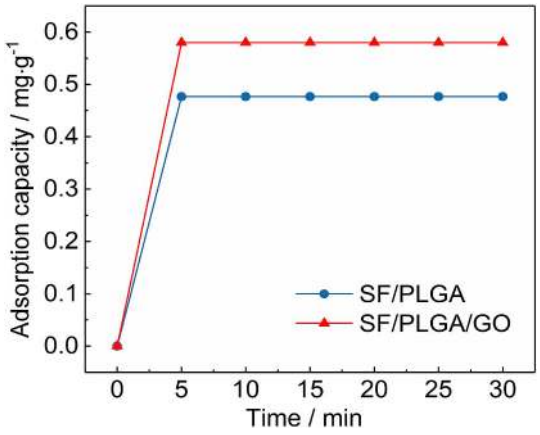

Fig. 8. Adsorption curves of microfiber mats.

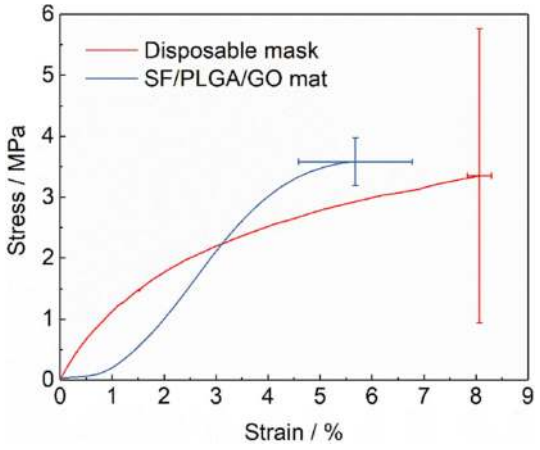

Fig. 9. The stress-strain curves of disposable mask and SF/PLGA/GO mat.

repellency, as shown in Fig. 2. It indicates that the SF/PLGA/GO microfiber mat does not provide a suitable moist environment for bacterial growth. In addition, many reports indicate that GO holds great promise for combating microbial growth [63,64].

3.8. The adsorption capacity of the microfiber mats

In practical applications, carrying drugs may also be required for protective fabrics. Therefore, the adsorption capacities of microfiber mats are investigated. The relationships between the amount of Reactive Dye Red 261 adsorption and water contact time (C_0 = 10 mg/mL^{-1}) at room temperature are presented in Fig. 8. The SF/PLGA/GO mat has a larger adsorption capacity than the SF/PLGA mat and can reach equilibrium around 5 min. The SF/PLGA/GO mat has greater absorptivity to Reactive Dye Red 261, indicating that the prepared SF/PLGA/GO mat can carry drugs for clinical applications where necessary.

3.9. Discussion

The stress-strain curves of the disposable commodity masks were measured, as shown in Fig. 9. The tensile strength of the SF/PLGA/GO mat prepared here is almost equal to the tensile strength of the commodity disposable mask. And we aim to fabricate the disposable textiles, such as disposable masks or outerwear, which are often used in labs and hospitals. It can also be used for a filter film last a shorter time. Fig. 10 shows the images of already established products (the disposable commodity masks) and our SF/PLGA/GO mat. It can be seen that the commodity masks' porosity is large. Our fabricated mats are more capable of filtering fine particulate pollutants and can be self-degrade after disposable. Environment protection is now an important task for humanity. Currently, protective textiles on the market are mainly chemical fiber products that cannot or are not easily degraded naturally. At present, due to the incomplete recycling of used textiles, it will lead to environmental pollution and is not conducive to sustainable development. Therefore, it is very necessary to develop degradable protective materials.

4. Conclusion

The biodegradable SF/PLGA and SF/PLGA/GO microfiber mats were successfully fabricated by electrospinning. The basic physical properties of these mats are tested and demonstrated. The SF/PLGA/GO mat achieve higher ultimate stress, Young's modulus and thermal stability. The ultimate stress of SF/PLGA/GO mat is 3.71 MPa, which is 53% higher than the SF/PLGA mat, indicating that SF/PLGA/GO microfiber mat has good physical properties and can meet the requirements for strength for protective fabrics. The fabricated SF/PLGA/GO microfiber mat obtained greater surface area and pore volume and had a smaller pore size than the SF/PLGA mat. Its diameter is 4 ~ 10 nm, far smaller than the sizes of particulate pollutants and pathogenic particles, which results in effective prevention of these pollutants. Its large surface area of 2.63 m^2 g^{-1} and pore volume of 7.09 × 10^{-3} cm^3 g^{-1} are effective for breathability. Therefore, the fabricated SF/PLGA/GO microfiber mat has great application potentials for protective fabrics.

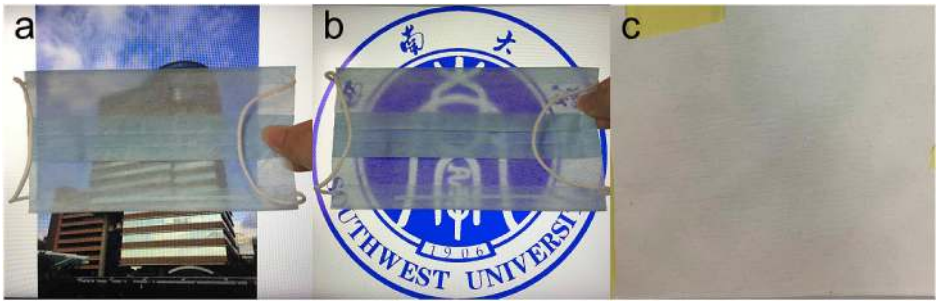

Fig. 10. The images of the disposable commodity masks (a, b), and (c) is our SF/PLGA/GO mat.

Declaration of competing interest

The authors declare that they have no conflict of interest.

Acknowledgments

PolyU's Mainland University Joint Supervision Scheme (G-SB0E) & GRF Funding (15301017).

Appendix A. Supplementary data

Supplementary data to this article can be found online at https://doi.org/10.1016/j.msec.2019.110308.

References

[1] X. Li, C. Wang, X.H. Huang, T.H. Zhang, X.F. Wang, M.H. Min, L.M. Wang, H.L. Huang, B.S. Hsiao, Anionic surfactant-triggered steiner geometrical poly(vinylidene fluoride) nanofiber/nanonet air filter for efficient particulate matter removal, ACS Appl. Mater. Interfaces 10 (49) (2018) 42891–42904.
[2] Y.Y. Zhang, S. Yuan, X. Feng, H.W. Li, J.W. Zhou, B. Wang, Preparation of nanofibrous metal-organic framework filters for efficient air pollution control, J. Am. Chem. Soc. 138 (18) (2016) 5785–5788.
[3] A.H. Mamaghani, F. Haghighat, C.S. Lee, Photocatalytic oxidation technology for indoor environment air purification: the state-of-the-art, Appl. Catal. B Environ. 203 (2017) 247–269.
[4] C. Liu, P.C. Hsu, H.W. Lee, M. Ye, G.Y. Zheng, N.A. Liu, W.Y. Li, Y. Cui, Transparent air filter for high-efficiency PM2.5 capture, Nat. Commun. 6 (2015) 9.
[5] R.F. Zhang, C. Liu, P.C. Hsu, C.F. Zhang, N. Liu, J.S. Zhang, H.R. Lee, Y.Y. Lu, Y.C. Qiu, S. Chu, Y. Cui, Nanofiber air filters with high-temperature stability for efficient PM2.5 removal from the pollution sources, Nano Lett. 16 (6) (2016) 3642–3649.
[6] S.X. Wang, C.C. Yap, J.T. He, C. Chen, S.Y. Wong, X. Li, Electrospinning: a facile technique for fabricating functional nanofibers for environmental applications, Nanotechnol. Rev. 5 (1) (2016) 51–73.
[7] Y. Wang, X. Zhao, X. Jiao, D. Chen, Electrospun filters for air filtration: comparison with existing air filtration technologies, in: M.L. Focarete, C. Gualandi, S. Ramakrishna (Eds.), Filtering Media by Electrospinning: Next Generation Membranes for Separation Applications, Springer International Publishing, Cham, 2018, pp. 47–67.
[8] D. Weiss, D. Skrybeck, H. Misslitz, D. Nardini, A. Kern, K. Kreger, H.W. Schmidt, Tailoring supramolecular nanofibers for air filtration applications, ACS Appl. Mater. Interfaces 8 (23) (2016) 14885–14892.
[9] J.W. Xu, C. Liu, P.C. Hsu, K. Liu, R.F. Zhang, Y.Y. Liu, Y. Cui, Roll-to-Roll transfer of electrospun nanofiber film for high-efficiency transparent air filter, Nano Lett. 16 (2) (2016) 1270–1275.
[10] Y.J. Yang, S.C. Zhang, X.L. Zhao, J.Y. Yu, B. Ding, Sandwich structured polyamide-6/polyacrylonitrile nanonets/bead-on-string composite membrane for effective air filtration, Separ. Purif. Technol. 152 (2015) 14–22.
[11] N. Bhardwaj, S.C. Kundu, Electrospinning: a fascinating fiber fabrication technique, Biotechnol. Adv. 28 (3) (2010) 325–347.
[12] Y. Liao, C.H. Loh, M. Tian, R. Wang, A.G. Fane, Progress in electrospun polymeric nanofibrous membranes for water treatment: fabrication, modification and applications, Prog. Polym. Sci. 77 (2018) 69–94.
[13] L.L. Min, H. Pan, S.Y. Chen, C.Y. Wang, N. Wang, J. Zhang, Y. Cao, X.Y. Chen, X. Hou, Recent progress in bio-inspired electrospun materials, Composites Communications 11 (2019) 12–20.
[14] H. Narayana, J.L. Hu, B. Kumar, S.M. Shang, M. Ying, R.J. Young, Designing of advanced smart medical stocking using stress-memory polymeric filaments for pressure control and massaging, Materials Science & Engineering C-Materials for Biological Applications 91 (2018) 263–273.
[15] S. Thenmozhi, N. Dharmaraj, K. Kadirvelu, H.Y. Kim, Electrospun nanofibers: new generation materials for advanced applications, Materials Science and Engineering B-Advanced Functional Solid-State Materials 217 (2017) 36–48.
[16] E. Correa, M.E. Moncada, O.D. Gutierrez, C.A. Vargas, V.H. Zapata, Characterization of polycaprolactone/rGO nanocomposite scaffolds obtained by electrospinning, Materials science & engineering. C, Materials for biological applications 103 (2019) 109773.
[17] M. Heidari, S.H. Bahrami, M. Ranjbar-Mohammadi, P.B. Milan, Smart electrospun nanofibers containing PCL/gelatin/graphene oxide for application in nerve tissue engineering, Materials science & engineering, C, Materials for biological applications 103 (2019) 109768.
[18] L.D. Koh, Y. Cheng, C.P. Teng, Y.W. Khin, X.J. Loh, S.Y. Tee, M. Low, E.Y. Ye, H.D. Yu, Y.W. Zhang, M.Y. Han, Structures, mechanical properties and applications of silk fibroin materials, Prog. Polym. Sci. 46 (2015) 86–110.
[19] C.B. Borkner, M.B. Elsner, T. Scheibel, Coatings and films made of silk proteins, ACS Appl. Mater. Interfaces 6 (18) (2014) 15611.
[20] C. Vepari, D.L. Kaplan, Silk as a biomaterial, Prog. Polym. Sci. 32 (8) (2007) 991–1007.
[21] S.M. Shang, L. Zhu, J.T. Fan, Physical properties of silk fibroin/cellulose blend films regenerated from the hydrophilic ionic liquid, Carbohydr. Polym. 86 (2) (2011) 462–468.
[22] E. Ko, J.S. Lee, H. Kim, S.Y. Yang, D. Yang, K. Yang, J. Lee, J. Shin, H.S. Yang, W. Ryu, S.W. Cho, Electrospun silk fibroin nanofibrous scaffolds with two-stage hydroxyapatite functionalization for enhancing the osteogenic differentiation of human adipose-derived mesenchymal stem cells, ACS Appl. Mater. Interfaces 10 (9) (2018) 7614–7625.
[23] X. Wang, B.S. Hsiao, Electrospun nanofiber membranes, Current Opinion in Chemical Engineering 12 (2016) 62–81.
[24] C.T. Kenry, Lim, Nanofiber technology: current status and emerging developments, Prog. Polym. Sci. 70 (2017) 1–17.
[25] G.H. Altman, F. Diaz, C. Jakuba, T. Calabro, R.L. Horan, J. Chen, H. Lu, J. Richmond, D.L. Kaplan, Silk-based biomaterials, Biomaterials 24 (3) (2003) 401–416.
[26] S.M. Shang, L. Zhu, J.T. Fan, Intermolecular interactions between natural polysaccharides and silk fibroin protein, Carbohydr. Polym. 93 (2) (2013) 561–573.
[27] H. Tao, D.L. Kaplan, F.G. Omenetto, Silk materials - a road to sustainable high technology, Adv. Mater. 24 (21) (2012) 2824–2837.
[28] N. Lin, L. Cao, Q. Huang, C. Wang, W. Yan, Z. Jin, X.Y. Liu, Functionalization of silk fibroin materials at mesoscale, Adv. Funct. Mater. 26 (48) (2016).
[29] S. Stankovich, D.A. Dikin, R.D. Piner, K.A. Kohlhaas, A. Kleinhammes, Y. Jia, W. Yue, S.B.T. Nguyen, R.S. Ruoff, Synthesis of graphene-based nanosheets via chemical reduction of exfoliated graphite oxide, Carbon 45 (7) (2007) 1558–1565.
[30] W.S.H. Jr, R.E. Offeman, Preparation of graphitic oxide, J. Am. Chem. Soc. 80 (6) (1958) 1339.
[31] L. Gan, S. Shang, C.W.M. Yuen, S.-x. Jiang, Graphene nanoribbon coated flexible and conductive cotton fabric, Compos. Sci. Technol. 117 (2015) 208–214.
[32] G. Wei, The chemistry of graphene oxide, Chem. Soc. Rev. 39 (1) (2009) 228–240.
[33] A. Gulzar, P. Yang, F. He, J. Xu, D. Yang, L. Xu, M.O. Jan, Bioapplications of graphene constructed functional nanomaterials, Chem. Biol. Interact. 262 (2016) 69–89.
[34] D. Ege, A.R. Kamali, A.R. Boccaccini, Graphene oxide/polymer-based biomaterials, Adv. Eng. Mater. 19 (12) (2017).
[35] M.Q. Wang, C.Y. Wang, Y.J. Song, C.H. Zhang, L. Shao, Z.X. Jiang, Y.D. Huang, Facile method to functionalize graphene oxide nanoribbons and its application to Poly(p-phenylene benzobisoxazole) composite, Compos. Sci. Technol. 165 (2018) 124–130.
[36] W.X. Hou, Y. Gao, J. Wang, D.J. Blackwood, S. Teo, Nanodiamond decorated graphene oxide and the reinforcement to epoxy, Compos. Sci. Technol. 165 (2018) 9–17.
[37] S. Tadepalli, H. Hamper, H.P. Sang, S. Cao, R.R. Naik, S. Singamaneni, Adsorption behavior of silk fibroin on amphiphilic graphene oxide, ACS Biomater. Sci. Eng. 2 (7) (2016).
[38] W. Xie, S. Tadepalli, S.H. Park, A. Kazemi-Moridani, Q. Jiang, S. Singamaneni, J.H. Lee, Extreme mechanical behavior of nacre-mimetic graphene-oxide and silk nanocomposites, Nano Lett. 18 (2) (2018) acs.nanolett.7b04421.
[39] Y. Luo, H. Shen, Y. Fang, Y. Cao, J. Huang, M. Zhang, J. Dai, X. Shi, Z. Zhang, Enhanced proliferation and osteogenic differentiation of mesenchymal stem cells on graphene oxide-incorporated electrospun poly(lactic-co-glycolic acid) nanofibrous mats, ACS Appl. Mater. Interfaces 7 (11) (2015) 6331.
[40] V. Stanic, A.C. Pierre, T.H. Etsell, R.J. Mikula, Preparation and characterization of GeS2, Polym. Eng. Sci. 53 (7) (2013) 1414–1429.
[41] C. Dionigi, T. Posati, V. Benfenati, A. Sagnella, A. Pistone, S. Bonetti, G. Ruani, F. Dinelli, G. Padeletti, R. Zamboni, A nanostructured conductive bio-composite of silk fibroin–single walled carbon nanotubes, J. Mater. Chem. B 2 (10) (2014) 1424–1431.
[42] C. Zhang, D. Song, L. Qiang, H. Xiao, D.L. Kaplan, H. Zhu, Flexibility regeneration of silk fibroin in vitro, Biomacromolecules 13 (7) (2012) 2148.
[43] M. Khan, H. Morikawa, Y. Gotoh, M. Miura, Z. Ming, Y. Sato, M. Iwasa, Structural characteristics and properties of Bombyx mori silk fiber obtained by different artificial forcibly silking speeds, Int. J. Biol. Macromol. 42 (3) (2008) 264–270.
[44] I. Cucchi, A. Boschi, C. Arosio, F. Bertini, G. Freddi, M. Catellani, Bio-based conductive composites: preparation and properties of polypyrrole (PPy)-coated silk fabrics, Synth. Met. 159 (3) (2009) 246–253.
[45] HyoungJoon JIN, Jaehyung PARK, Vassilis KARAGEORGIOU, UngJin KIM, Regina VALLUZZI, Water-stable silk films with reduced β-sheet content, Adv. Funct. Mater. 15 (8) (2005) 1241–1247.
[46] K. Kim, S. Coh, L.Z. Tan, W. Regan, J.M. Yuk, E. Chatterjee, M.F. Crommie, M.L. Cohen, S.G. Louie, A. Zettl, Raman spectroscopy study of rotated double-layer graphene: misorientation-angle dependence of electronic structure, Phys. Rev. Lett. 108 (24) (2012) 246103.
[47] K.T. Nguyen, D. Abdula, C.L. Tsai, M. Shim, Temperature and gate voltage dependent Raman spectra of single-layer graphene, ACS Nano 5 (6) (2011) 5273–5279.
[48] J. Chen, Y. Zhang, M. Zhang, B. Yao, Y. Li, L. Huang, C. Li, G. Shi, Water-enhanced oxidation of graphite to graphene oxide with controlled species of oxygenated groups, Chem. Sci. 7 (3) (2016) 1874–1881.
[49] K.N. Kudin, B. Ozbas, H.C. Schniepp, R.K. Prud'homme, I.A. Aksay, R. Car, Raman spectra of graphite oxide and functionalized graphene sheets, Nano Lett. 8 (1) (2008) 36–41.
[50] H. Liang, L. Chun, Y. Wenjing, S. Gaoquan, Strong composite films with layered structures prepared by casting silk fibroin-graphene oxide hydrogels, Nanoscale 5 (9) (2013) 3780–3786.
[51] X.M. Yang, S.M. Shang, L.A. Li, Layer-Structured poly(vinyl alcohol)/graphene oxide nanocomposites with improved thermal and mechanical properties, J. Appl. Polym. Sci. 120 (3) (2011) 1355–1360.
[52] X. Yang, S. Shang, L. Li, Layer-structured poly(vinyl alcohol)/graphene oxide

nanocomposites with improved thermal and mechanical properties, J. Appl. Polym. Sci. 120 (3) (2011) 1355–1360.
[53] G. Mittal, K.Y. Rhee, V. Miskovic-Stankovic, D. Hui, Reinforcements in multi-scale polymer composites: processing, properties, and applications, Compos. B Eng. 138 (2018) 122–139.
[54] S.M. Shang, L. Gan, C.W.M. Yuen, S.X. Jiang, N.M. Luo, The synthesis of graphene nanoribbon and its reinforcing effect on poly (vinyl alcohol), Compos. Appl. Sci. Manuf. 68 (2015) 149–154.
[55] M. Zhao, L.H. Meng, L.C. Ma, L.N. Ma, X.B. Yang, Y.D. Huang, J.E. Ryu, A. Shankar, T.X. Li, C. Yan, Z.H. Guo, Layer-by-layer grafting CNTs onto carbon fibers surface for enhancing the interfacial properties of epoxy resin composites, Compos. Sci. Technol. 154 (2018) 28–36.
[56] X.Q. Yan, J. Yang, F. Chen, L. Zhu, Z.Q. Tang, G. Qin, Q. Chen, G.M. Chen, Mechanical properties of gelatin/polyacrylamide/graphene oxide nanocomposite double-network hydrogels, Compos. Sci. Technol. 163 (2018) 81–88.
[57] X. Zhao, Y. Li, T. Hua, P. Jiang, X. Yin, J. Yu, B. Ding, Cleanable air filter transferring moisture and effectively capturing PM2. 5, Small 13 (11) (2017) 1603306.
[58] J. Xu, C. Liu, P.-C. Hsu, K. Liu, R. Zhang, Y. Liu, Y. Cui, Roll-to-roll transfer of electrospun nanofiber film for high-efficiency transparent air filter, Nano Lett. 16 (2) (2016) 1270–1275.
[59] F. Li, W.H. Li, M. Farzan, S.C. Harrison, Structure of SARS coronavirus spike receptor-binding domain complexed with receptor, Science 309 (5742) (2005) 1864–1868.
[60] D.E. Swayne, Avian Influenza, John Wiley & Sons, 2009.
[61] E.P. Ivanova, Nanoscale Structure and Properties of Microbial Cells Surfaces, Nova Science Publishers, 2007.
[62] 14117, M. Eddaoudi, Characterization of porous solids and Powders: surface area, pore size and density by S. Lowell (Quantachrome instruments, boynton beach), J. Am. Chem. Soc. 127 (40) (2005) 14117.
[63] X. Zou, L. Zhang, Z. Wang, Y. Luo, Mechanisms of the antimicrobial activities of graphene materials, J. Am. Chem. Soc. 138 (7) (2016) 2064.
[64] S. Szunerits, R. Boukherroub, Antibacterial activity of graphene-based materials, J. Mater. Chem. B 4 (43) (2016).